Eur. Phys. J. A **29**, 353–361 (2006)
DOI 10.1140/epja/i2006-10099-3

THE EUROPEAN PHYSICAL JOURNAL A

Study of spectator tagging in the reaction np → ppπ^- with a deuteron beam

The COSY-TOF Collaboration

M. Abdel-Bary[4], K.-Th. Brinkmann[1], H. Clement[3], E. Doroshkevich[3], S. Dshemuchadse[1], A. Erhardt[3], W. Eyrich[2], H. Freiesleben[1], A. Gillitzer[4], R. Jäkel[1], L. Karsch[1], K. Kilian[4], E. Kuhlmann[1,a], K. Möller[5], H.P. Morsch[4], L. Naumann[5], N. Paul[4], C. Pizzolotto[2], J. Ritman[4], E. Roderburg[4], P. Schönmeier[1,b], W. Schroeder[2], M. Schulte-Wissermann[1], G.Y. Sun[1], A. Teufel[2], A. Ucar[4], G.J. Wagner[3], M. Wagner[2], P. Wintz[4], P. Wüstner[4], and P. Zupranski[6]

[1] Institut für Kern- und Teilchenphysik, Technische Universität Dresden, D-01062 Dresden, Germany
[2] Physikalisches Institut, Universität Erlangen, D-91058 Erlangen, Germany
[3] Physikalisches Institut, Universität Tübingen, D-72076 Tübingen, Germany
[4] Institut für Kernphysik, Forschungszentrum Jülich, D-52425 Jülich, Germany
[5] Institut für Kern- und Hadronenphysik, Forschungszentrum Rossendorf, D-01314 Dresden, Germany
[6] Andrzej Soltan Institute for Nuclear Studies, PL-00681, Warsaw, Poland

Received: 16 May 2006 / Revised: 7 September 2006 /
Published online: 22 September 2006 –
Communicated by M. Garçon

Abstract. The reaction $dp \to ppp\pi^-$ has been studied in a kinematically complete experiment at a single beam momentum $p_d = 1.85\,\mathrm{GeV}/c$ ($T = 759\,\mathrm{MeV}$). All four ejectiles have been detected in the large-acceptance time-of-flight spectrometer COSY-TOF. We analyzed the data along the lines of the spectator model as a means to isolate the quasi-free $np \to pp\pi^-$ reaction. The spectator proton was identified by its momentum and flight direction thus yielding access to the associated Fermi motion of the bound neutron. A comparison is carried out with Monte Carlo simulations based on two different parameterizations of the deuteron wave function. Up to a Fermi momentum of roughly $150\,\mathrm{MeV}/c$ no significant deviations between experimental and simulated data of various observables were found from which we conclude that the deuteron can indeed be taken as a valid substitute for the neutron.

PACS. 13.75.Cs Nucleon-nucleon interactions – 25.10.+s Nuclear reactions involving few-nucleon systems – 29.20.Dh Storage rings – 29.90.+r Other topics in elementary-particle and nuclear physics experimental methods and instrumentation

1 Introduction

Pion producing reactions have been known to dominate the low-energy regime in strong-interaction physics for a long time and as such are fundamental for the understanding of the NN-force. Assuming isospin invariance, all single pion production reactions in NN collisions with three-body final states can be decomposed into a sum of at most two out of three elementary cross-sections σ_{I_i,I_f} [1] with I_i and I_f denoting the isospin of the NN system in the initial and final state, respectively. Starting from the pp-entrance channel two reactions are possible, $pp \to pp\pi^0$ and $pp \to pn\pi^+$, yielding, respectively, σ_{11} and $\sigma_{11} + \sigma_{10}$. The third, isoscalar cross-section, σ_{01}, can only be determined through a measurement of $np \to NN\pi$ reactions as, *e.g.*, $np \to pp\pi^-$, which is given by $\sigma_{01}+\sigma_{11}$. Since neutron targets are not available, measurements of this reaction in the past have either been performed by use of a neutron beam [2–7] or a deuterium target [8–12]. In case of the latter, the analysis is based on the validity of the spectator model which assumes that 1) the proton in the deuteron is a spectator, influencing the reaction only in terms of the associated Fermi motion of the bound neutron, and 2) that the matrix element for quasi-free pion production from a bound neutron is identical to that for free pion production from an unbound neutron at the same two-body energy and momentum transfer. A way to check the first assumption will require the detection of the spectator proton, which, however, in most cases was not attempted, since its very low energy of only a few MeV prevents it

[a] e-mail: e.kuhlmann@physik.tu-dresden.de
[b] *Present address:* Physikalisches Institut, Universität Erlangen, D-91058 Erlangen, Germany.

from escaping the target region and/or reaching a suitable detection unit.

First experiments on π^--producing reactions on nuclear targets were started in the late seventies [8], where in a series of p-nucleus scattering experiments charged pions were detected at selected angles in the range 22.5°–135°. No attempts to extract the contributions of the np-entrance channel were made. Some 10 years later a group at TRIUMF initiated the first dedicated experiments [11, 12], where in order to bypass the difficulties of low-energy spectator detection, the final-state protons were restricted to the $^1S_0$, the "diproton" state; this was achieved by selecting only those events with proton pairs that show small momentum differences within a narrow solid angle. By cutting in this way into the kinematically allowed phase space, however, it is obvious, that only a somewhat truncated picture of the true process can be obtained. Thus, detecting also the spectator proton is the only solution, and most recently some progress has been made in internal target experiments at CELSIUS [13] and COSY [14,15], where windowless cluster jet or pellet targets were employed and spectator protons with energies as low as 2 MeV could be observed in specifically designed telescopes placed in the backward region of the target.

In order to avoid the necessity to detect low-energy spectator nucleons at all, one might use a deuteron beam hitting a proton target where one can expect the spectator proton to leave the interaction zone with momenta around half the beam momentum and close to the beam direction. Thus, to shed more light onto the possibilities of the spectator tagging method, we have initiated a comprehensive investigation of the reaction $dp \to pp\pi^- p_s$ using the external deuteron beam of the cooler synchrotron COSY at the FZ Jülich/Germany. In addition to the fast spectator denoted as p_s one finds in this reaction charged reaction products only which in principle can all be detected with our large-acceptance time-of-flight spectrometer COSY-TOF. By choosing a single deuteron momentum of $p_d = 1.85\,\mathrm{GeV}/c$ we could cover as a consequence of the varying Fermi momentum an excess energy range ΔQ spanning roughly 100 MeV above threshold. The goals were twofold: 1) we wanted to measure angular and momentum distributions of all participating ejectiles as well as determine the amount of final-state interaction effects in the proton pair and set up Q-dependent Dalitz plots and 2) on a more technical basis we tried to perform a detailed performance check of the proposed method of spectator tagging and study its possibilities. In this paper we will present the results obtained for the latter goal deduced from events where all four ejectiles were detected. Results on cross-sections, angular and momentum distributions will be the subject of a forthcoming paper which will be based on the analysis of a larger data sample containing also those events where one of the four particles escaped detection but could be reconstructed through energy and momentum conservation.

To our knowledge, there is but one recent report on pion production through use of a deuteron beam, which was carried out at $3.34\,\mathrm{GeV}/c$ [16]; data extracted from ^{4}He-induced reactions were also given. In that experiment the hydrogen bubble chamber at the JINR in Dubna/Russia was used serving both as a target and as a detector with full solid-angle coverage. In some cases significant asymmetries in the angular distributions of the spectator particles were found, a result that shall be scrutinized through comparison with the present study.

2 Experimental procedure

2.1 Apparatus

The experiment was carried out with the time-of-flight spectrometer COSY-TOF set up at an external beamline of the 2.5 GeV proton synchrotron COSY. Charged particles escaping from the reaction zone into the forward direction were detected in a multi-layer scintillator hodoscope by measuring their flight time as well as direction. The performance of the whole system is described in a series of papers on photon [17], meson [18] and hyperon production [19], hence we will give only a short overview. A schematic sketch of the spectrometer showing the locations of the main components, the Barrel, Ring, and Quirl detector, as well as the target region with its miniaturized liquid-hydrogen target and start detector system is given in fig. 1. To prevent the reaction products from undergoing secondary reactions on their way from the target to the different detector modules, the entire apparatus is housed within a 3.3 m$\varnothing \times 4$ m steel tank evacuated to a pressure of 0.2 Pa. Deuterons were extracted from the COSY ring in a slow extraction mode. Their intensity typically was of the order of several 10^6/s, spills lasted up to 5 min. The beam was focussed onto a liquid-hydrogen target with dimensions 6 mm$\varnothing \times 4$ mm. Its front and rear ends were closed by 0.9 μm thin hostaphan foils [20]. Scintillator veto detectors with central holes of various sizes were located 260, 51 and 3.5 cm upstream of the target, respectively. They helped to define the beam spot in the center of the target to an area with a diameter of $d = 3.0$ mm. Charged particles emitted from the target into the forward hemisphere first had to traverse a circular, two-layered plastic scintillator of a total thickness of 2 mm which served as a start detector for the time-of-flight measurement. Each of its layers is axially segmented giving an overall ϕ-resolution of 15° [21].

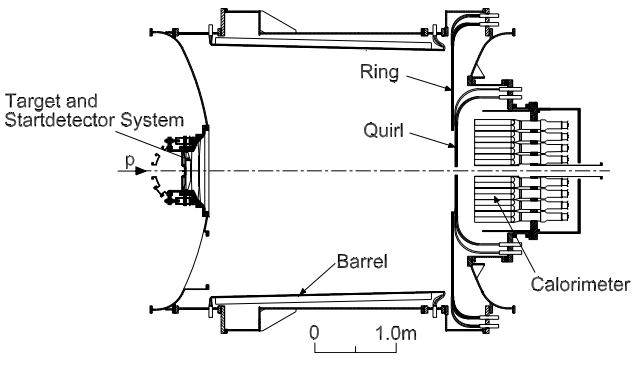

Fig. 1. Sketch of the COSY-TOF spectrometer.

The signals obtained from two sets of scintillating fiber hodoscopes placed 10 and 20 cm behind the target were used for track reconstruction. After a flight path of up to 3 m, the reaction products hit the 3-component scintillator hodoscope. The circular, 3-layer Quirl and Ring detector components of the endcap are both built according to the same layout [22]. The first layer in the Quirl is made from 48 wedge-like scintillators, followed by two layers with 24 left and 24 right wound elements, each one cut along an Archimedian spiral. Thus each element in a given layer is subjected to the same particle flux. In central projection a net-like pattern is formed consisting of more than 1000 triangular pixels. A central hole of radius $r = 4.2$ cm is left for the beam, the outer radius of the Quirl is 58 cm. The three layers in the Ring are made from 96 wedges and 2×48 left and right wound Archimedian spirals, the inner (outer) radius is 56.8 (154) cm, respectively. The Barrel consists of 96 scintillator bars, mounted to the inside of the tank. Each bar of 2.85 m length has a cross-section of size thickness $\times$ width = 15 mm $\times$ 96 mm and is read out from both ends [23]. A calorimeter made from 84 scintillator blocks of hexagonal shape and 45 cm length is mounted behind the endcap and covers roughly the same solid angle as the Quirl [24]. In the present study, however, no use was made of this component.

2.2 Principle of measurement and data analysis

With four charged particles to emerge from the $dp \to pp\pi^- p_s$ reaction, the main trigger condition was such as to require four hits in any of the stop scintillator modules, Quirl, Ring, and Barrel, in addition to at least one hit in the start scintillator. Each photomultiplier signal was then used for energy loss as well as time-of-flight measurement. To this end, the analog signals were digitized in Fastbus-QDC modules, the timing signals were obtained from leading-edge–type discriminators and converted in Fastbus TDCs. Both measurements yield the particle velocity β. From the particle's point of impact as well as the tracking information of the fiber hodoscopes, the flight direction was obtained from which two additional observables, θ and ϕ, can be deduced. The spatial resolution as found from the analysis of elastic scattering events was $\Delta\theta = 0.3°(0.5°)$ for particles reaching the endcap (the barrel), respectively, and $\Delta\phi = 1°$. Typical values obtained for the time resolution of the start-stop system were of the order of 0.5 ns (FWHM) which corresponds to about 2.5% of the average flight time of a $\beta = 0.5$ particle. The momentum 4-vector $\mathbb{P}$ of each detected particle could then be deduced from the measured observables β, θ, and ϕ by applying additional mass hypotheses. Actually, four different hypotheses had to be tested with either one of the detected particles being a π^-. To find the correct assignment for each event, various methods as, *e.g.*, momentum conservation, missing mass and invariant mass analyses were probed and a careful comparison with results obtained from Monte Carlo simulations was performed, as will be outlined below.

In order to find θ, ϕ and β for each particle, several steps in calibrating the detector had to be performed such as pedestal subtraction in the QDC spectra, walk correction for each TDC entry and a determination of the channel width of each TDC module, which in some cases deviated from the preset value of 100 ps/channel by up to 10%. The most critical part was the determination of the TDC offsets arising from variations in the signal arrival times which were due to different cable lengths and varying transit times in the photomultiplier tubes and electronic modules [18]. These offsets were determined by firstly comparing overlapping, but otherwise identical channels as, *e.g.*, neighboring elements in the start detector or overlap regions from left- and right-wound elements in the endcap. Thus, detector offsets of the Quirl and Ring elements could be matched to each other. In a second step, the offsets of all components as well as the absolute time scale were fixed by analyzing data from *dp* elastic scattering. This binary reaction with its unique kinematics and sizeable cross-section was repeatedly measured in separate runs with an adjusted trigger condition.

Since a wide range in excess energy ΔQ was covered in the present experiment the detector acceptance also showed some variation. For large Q-values some fraction of π^--mesons were emitted into the backward hemisphere and thus could not be detected by the spectrometer which only spans a polar angular range up to roughly 60°. Another cut in acceptance originated from the charged particles' energy loss in the various detector layers resulting in a low β-threshold of $\beta \approx 0.35$ for π^--mesons and $\beta \approx 0.5$ for protons. Yet we still obtained an overall acceptance for four-particle detection of the order of 35%.

The free $np \to pp\pi^-$ reaction has a threshold of $p_{thr}(2N) = 0.788\,\mathrm{GeV}/c$ corresponding to a bombarding energy of $T_{thr}(2N) = 287\,\mathrm{MeV}$, the respective values for the deuteron-induced reaction are $p_{thr}(3N) = 1.344\,\mathrm{GeV}/c$ and $T_{thr}(3N) = 432\,\mathrm{MeV}$. For the present experiment we chose a deuteron momentum of $p_d = 1.85\,\mathrm{GeV}/c$ which corresponds for the free np reaction to an excess energy of 42.9 MeV. Since the Fermi momentum within the deuteron induces an additional contribution, the total energy $\sqrt{s}$ in the pn-subsystem will vary from event to event and hence has to be determined for each event separately. The momentum distribution within the deuteron with its s- and d-wave components can be calculated by using the PARIS potential and is shown in fig. 2 with a maximum near $40\,\mathrm{MeV}/c$ and a mean value close to $100\,\mathrm{MeV}/c$ [25,26].

As has been stated before, the validity of the spectator model is based on two assumptions, namely 1) the proton in the deuteron can be regarded as an unaffected spectator staying on-shell throughout the reaction and 2) the matrix element for quasi-free pion production from a bound neutron is identical to that for free pion production from an unbound neutron. A schematic representation of such a process is shown in fig. 3 where a fast deuteron with 4-momentum components $(E_d, \vec{p}_d)$ fragments into an on-shell spectator proton p_s with roughly half the beam momentum and an off-shell neutron which

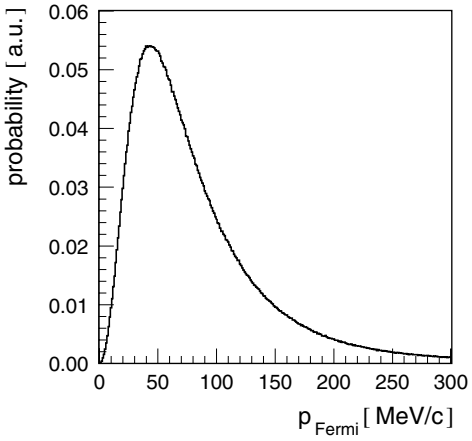

Fig. 2. Momentum distribution of the nucleons within the deuteron as calculated from the PARIS potential.

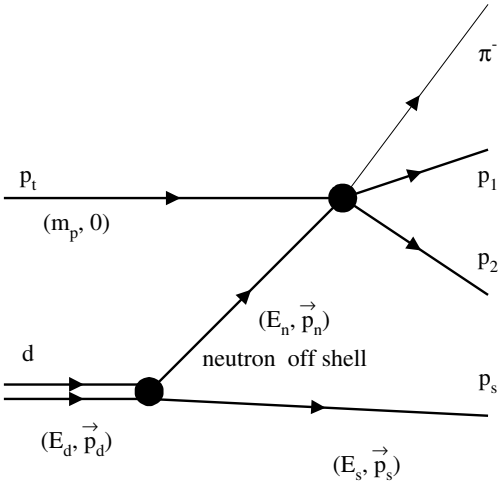

Fig. 3. Schematic representation of the reaction $dp \to pp\pi^- p_s$ in the laboratory system showing an unaffected spectator proton p_s escaping with 4-momentum components $(E_s, \vec{p}_s)$ and an off-shell neutron initiating the $np \to pp\pi^-$ reaction (see text).

in turn hits the target proton p_t thereby producing two protons and a π^-. At the core of the ensuing analysis lies the information gathered from the spectator proton. Within the spectator model this particle gives a direct measure of the Fermi momentum carried by the off-shell neutron at the time of the np reaction. By measuring the spectator momentum $\vec{p}_s$ and applying a subsequent transformation into the deuteron center-of-mass (DCM) system one finds its DCM momentum $\vec{p}_s^{\,*}$ and hence the DCM neutron momentum $\vec{p}_n^{\,*} = -\vec{p}_s^{\,*} = \vec{p}_{Fermi}$. The total energy of the spectator proton is given by $E_s^* = \sqrt{m_p^2 + |\vec{p}_s^{\,*}|^2}$ from which one finds the total energy of the neutron as $E_n^* = m_d - E_s^*$. Here the asterisks denote DCM components, m_p and m_d the free proton and deuteron masses. Even for a spectator proton at rest ($E_s^* = m_p$) the neutron necessarily is off-shell due to the binding energy of the deuteron. In general cases the mass of the neutron is given as $\hat{m}_n = \sqrt{(E_n^*)^2 - |\vec{p}_s^{\,*}|^2}$ which

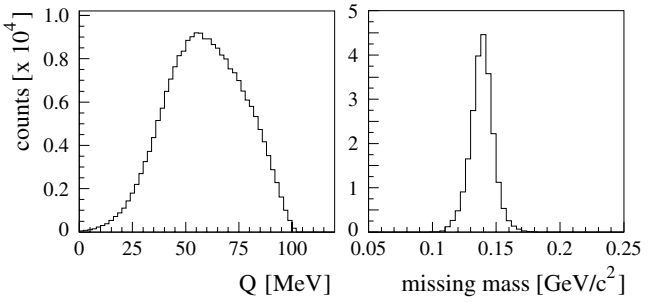

Fig. 4. Left: Range of excess energies covered in the present experiment at a single deuteron momentum $p_d = 1.85\,\mathrm{GeV}/c$. Right: missing mass spectrum of reconstructed quasi-free $np \to pp\pi^-$ events where projectile mass and projectile momentum varied from event to event.

can get as low as $0.8\,\mathrm{GeV}/c^2$. As a side effect this result induces an upper limit in excess energy Q given as $Q = \sqrt{(m_p + \hat{m}_n)^2 + 2 \cdot T_n m_p} - 2 \cdot m_p - m_\pi$.

The identification of the spectator proton was performed in several steps. With a beam momentum below the threshold for $\pi^+\pi^-$-production, any 4-hit event apart from accidentals could only result from the $dp \to pp\pi^- p_s$ reaction. Thus, in the first step, the pion had to be isolated by starting from four possible hypotheses, *i.e.* the pion being particle 1, 2, 3, or 4. For each case, the sums of longitudinal and transversal momentum components p_L and p_T were calculated. As the most probable assignment we chose the one where the sums were closest to the ones given from kinematics, namely $p_L = p_d$ and $p_T = 0$. The spectator proton was then identified as the particle which was detected closest to the beam axis with momentum near $p_d/2$. In a complementary approach we assigned 3 out of 4 particles to be a proton and for each hypothesis we calculated the missing mass m_X of the remaining particle. As the correct hypothesis we took the one where m_X was closest to the π^- mass and then identified the spectator as described above. By combining both methods it was possible to extract very clean event samples.

By transformation of the spectator momentum vector $\vec{p}_s$ into the DCM, the neutron momentum $\vec{p}_n^{\,*}$ was determined as well as the "projectile" mass $\hat{m}_n$. We could deduce the effective neutron-beam momentum by application of the inverse transformation back into the laboratory system, which together with $\hat{m}_n$ allowed us to fix for each event the total energy of the quasi-free $np \to pp\pi^-$ reaction $\sqrt{s}$ and the excess energy Q. Since the reconstructed Fermi momentum differs from event to event, both $\sqrt{s}$ and Q vary as well. The range in Q is shown in fig. 4 (left), the most probable Q-values are around 50 MeV, maximum values are found near 100 MeV. This distribution which was derived from close to $2.2 \cdot 10^5$ $pp\pi^- p_s$ events shows a characteristic shoulder on the high-energy side followed by an almost abrupt descent towards the maximum Q-value. This shape is due to the Q-dependent rise in cross-section as will be shown by our Monte Carlo simulation presented in sect. 2.3.

As a final check of the quality of our analysis and the reliability in identifying for each event the correct spec-

tator proton we calculated again the π^- mass along the lines of a standard missing mass analysis. Here, however, the reaction under study was the quasi-free $pn \to ppX$ reaction with three particles in the exit channel whereas the spectator proton as the fourth particle only supplies information on beam momentum. Since the experiment covers 100 MeV in excess energy Q, one obtains missing mass distributions where the widths gradually rise with Q. To demonstrate the almost total lack of background events we show in fig. 4 (right) the overall pion missing mass distribution having a width of close to $20\,\mathrm{MeV}/c^2$ (FWHM).

2.3 Monte Carlo simulation

The analysis of our exerimental data samples was continuously accompanied by extensive Monte Carlo simulations. The main body of the program package essentially is the same as was already used in our earlier work [18,27,28]. The option to allow each simulated quasi-free $np \to pp\pi^-$ event to have different initial kinematical parameters, however, enters into the simulation as a new and very important point. To this end, the routine calling the CERNLIB random event generator GENBOD [29] had to be modified. In the usual case GENBOD is called for a specified N-body reaction with a fixed entrance channel at a given beam momentum and then generates momentum 4-vectors $\mathbb{P}_i$ for all ejectiles in the overall center-of-mass system as well as weight factors w_e reflecting the phase space density. Then the event is boosted into the laboratory system and each particle is tracked through the various active and passive parts along its flight path within the spectrometer. In the present case, we additionally had to incorporate into the Monte Carlo code the spectator particle with its varying internal momentum and we had to specify the neutron initial 4-momentum vector $\mathbb{P}_n$ along the lines as described in sect. 2.2.

The basic reaction to be simulated is $np \to pp\pi^-$. For each event, however, the actual start of GENBOD was preceded by a 3-fold call to a random number generator yielding 1) a random $\cos\theta^*$ out of the interval $[-1,+1]$, 2) a random ϕ^* out of the interval $[0,2\pi]$ and 3) a random momentum $|\vec{p}^{\,*}|/(\mathrm{MeV}\cdot c^{-1})$ out of the interval [0,400]. Homogeneous distributions were set up in the first two cases, the momentum distribution was folded with the Fermi distribution of the nucleons within the deuteron, as was already discussed in sect. 2.2 (see also fig. 2). We identify the three-component vector $|\vec{p}^{\,*}|$, $\cos\theta^*, \phi^*$ as well as the one pointing into the opposite direction with those of an np-pair within the deuteron in the DCM system. Transformation into the laboratory system then allows one to deduce the corresponding vectors for spectator and projectile particle within a fast-moving deuteron of momentum $p_d = 1.85\,\mathrm{GeV}/c$. The fact that in the laboratory system the flight direction of the projectile neutron deviates by a small angle from that of the beam deuteron is accounted for by a suitably chosen rotation such that the neutron's flight direction serves as the actual beam direction. After having fixed event by event the momentum vector for the "beam neutron" it is straightforward to perform the simulation for $np \to pp\pi^-$.

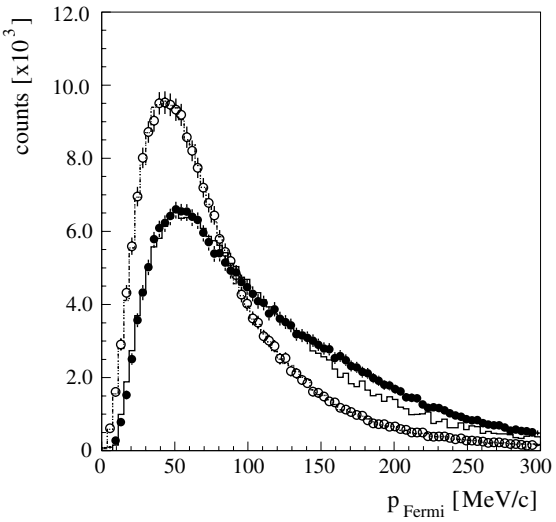

Fig. 5. Experimental momentum distribution of the neutron in the DCM system (solid dots) in comparison with Monte Carlo results. The solid histogram has been calculated from the PARIS potential, where the Q-dependent rise in cross-section was explicitly taken into account. When neglecting this dependence a distribution as given by the open circles was obtained. For comparison, the distribution resulting from the Hulthen function is also given (dash-dotted histogram).

In order to fulfill all kinematical constraints, any Monte Carlo simulation in its simplest form generates phase-space–distributed events, whereas any expected or known dynamical effects have to be added separately. This not only holds for angular distribution or final-state interaction effects, but —and this is specific for the present case— one also has to include the energy dependence of the cross-section into the simulation. Since the main purpose of the present paper aims at a critical test of the spectator model, we collected all necessary information from the literature. From studies of the $np \to pp\pi^-$ reaction, differential cross-sections as a function of the proton-proton invariant mass M_{pp} and the pion CM angle θ_π are known. A large set of integrated cross-sections and analyzing powers has been determined from threshold up to roughly $T_n = 1\,\mathrm{GeV}$ (see refs. [2–7]). Here, we mostly relied on the data obtained with a neutron beam at the PSI in Villigen/Switzerland [6].

In the range $\Delta Q = 10$–$100\,\mathrm{MeV}$ the cross-section rises by more than two orders of magnitude. To show the influence of this strong rise on the measured Fermi distribution we present in fig. 5 our $pp\pi^-$ data given by solid dots together with Monte Carlo results obtained with and without consideration of the energy dependence of the cross-section. To this end, the published cross-section [6] was parameterized as a function of Q by a 3rd-order polynomial yielding an additional weight factor w_Q. When neglecting w_Q, a Fermi distribution with a strong peak slightly below $50\,\mathrm{MeV}/c$ (given by open circles) was obtained which, however, does nowhere reproduce the experimental data.

This distribution actually is the result of two independent simulations lying almost on top of each other. The one calculated from the PARIS potential [25,26] and given by open circles can hardly be distinguished from the one calculated from the Hulthen wave function (dash-dotted histogram) given in a compact analytical form as [10]

$$\varphi(p_{Fermi}) = N \cdot \frac{\beta^2 - \alpha^2}{(p_{Fermi}^2 + \alpha^2) \cdot (p_{Fermi}^2 + \beta^2)}$$

with $\alpha(\beta) = 0.0456(0.260)\,\mathrm{GeV}/c$, respectively, and N denoting a normalization factor. We would like to point out that in cases like this where no differentiation between s- and d-wave components is asked for and where only momenta below $300\,\mathrm{MeV}/c$ have to be considered, the Hulthen function is quite sufficient, but much easier to handle than the full potential solution. When weighting the simulated events by $w_e \cdot w_Q$, the solid histogram is found which reproduces the experimental data up to a Fermi momentum of about $150\,\mathrm{MeV}/c$ in an almost perfect way. To get a more quantitative measure of the agreement we carried out a χ^2-fit of the Monte Carlo results to the experimental data in the range up to this limit and obtained a reduced $\chi^2/n_f = 34.5/37$ with n_f denoting the number of degrees of freedom. Here the statistical errors are far below the systematic ones of order 10% which are made up by an overall 7% uncertainty in cross-section [6], a 5% error in acceptance correction as well as 3.5% each for misinterpreted background events and wrong particle assignments. The simulation stays below the data for higher momenta, which will be discussed in the next section. We would like to mention that the normalization factor which served as the only free parameter in the fit will be the same in all of the following comparisons. Also in this case the results obtained from the PARIS potential and the Hulthen function are nearly indistinguishable.

3 Results and discussion

In the range covered by the present experiment the cross-section rises up to almost $400\,\mu$b, hence data with a high statistical significance could be obtained. In fig. 6 we show as a first example the angular distribution of the spectator protons in the DCM system together with Monte Carlo results. The experimental data given by the solid dots exhibit a strong peak at the far backward angles, a result which is nicely reproduced by the simulation (solid histogram). From a fit to the data in the $\cos\theta_s^*$ range $[-0.9, +0.9]$ we obtained a reduced $\chi^2/n_f = 47.4/38$. The various other histograms shown in the figure were obtained at different stages of the simulation. The dash-dotted histogram represents the start-up distribution assumed to be isotropic. Obviously, the distribution for the neutrons within the deuteron has to look the same. Due to the fact that at a deuteron beam momentum of $1.85\,\mathrm{GeV}/c$ we are not far from threshold, some of the backward neutrons will have too small momenta to initiate π^--production, hence the corresponding forward-going spectator protons will

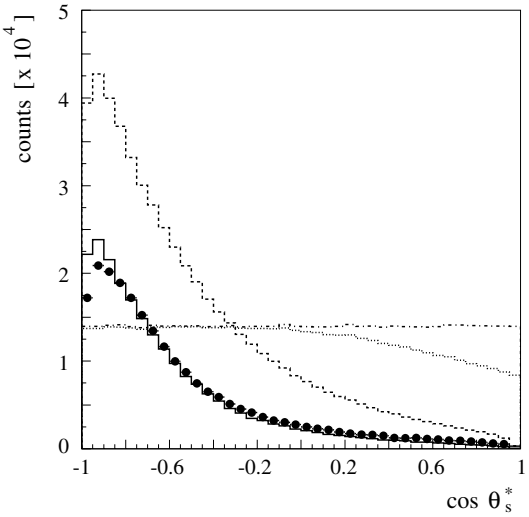

Fig. 6. Experimental angular distribution of the spectator proton in the deuteron center-of-mass system (solid dots) in comparison with Monte Carlo data as obtained at various stages of the simulation (see text).

not be seen in the reaction (dotted histogram). Weighting this adjusted distribution with the Q-dependent rise in cross-section as discussed before, the dashed histogram is found. When correcting for detector acceptance we finally arrive at the solid histogram.

We would like to point out that although the distribution is anything but isotropic, we have started our Monte Carlo simulation from just such a distribution. The strong rise in cross-section by more than a factor of 100 in the Q-excess range 10–100 MeV, however, leads to the observed strong peaking at backward spectator angles, which in turn reflects the dominance of the forward-going neutrons, where beam and Fermi momentum are in parallel thus allowing access to larger excess energies.

In the absence of such effects the angular distribution of spectator protons p_s in the DCM should be isotropic [10]. To check this claim we also analyzed the p_s angular distribution as deduced from events of the quasi-elastic scattering reaction $dp \rightarrow pnp_s$. At a neutron beam momentum around $1\,\mathrm{GeV}/c$ the cross-section for np elastic scattering is nearly constant over several hundred MeV/c [30,31]; Besliu *et al.* [30] report a value of 28.6 mb at $p_n = 1.25\,\mathrm{GeV}/c$, whereas from the work of Devlin *et al.* [31] on total cross-section measurements in the range 0.7–3.6 GeV/c one finds cross-sections of the order of 34 mb near $0.9\,\mathrm{GeV}/c$, where the contribution of inelastic processes can still be regarded as small. Events of this reaction could be observed in the range $\Delta\theta = 26°$–$57°$. A second trigger condition focussed on the detection of 3-hit events, but with a suppression factor of ten. Here the neutrons were identified by their leaving no trace in any of the preceding detector elements, but still having a finite detection probability of about 3% in the 15 mm thick scintillator slabs of the Barrel detector. This probability is even more enhanced due to the non-perpendicular impact angle. Yet, contrary to the almost constant detection

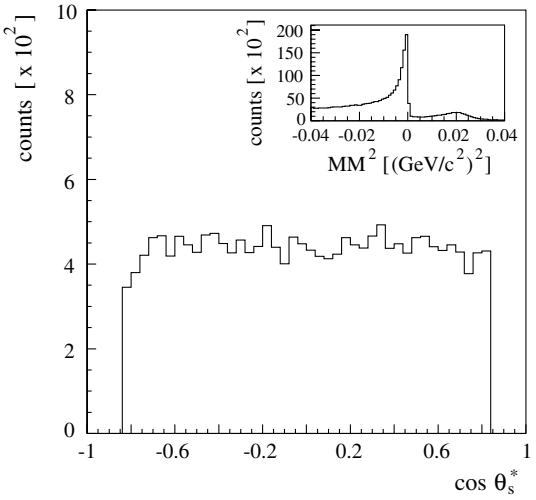

Fig. 7. Experimental angular distribution of the spectator protons in the DCM system as obtained from the $dp \rightarrow pnp_s$ quasi-elastic scattering reaction. The insert shows the squared missing mass distribution reconstructed from 3-hit events (see text).

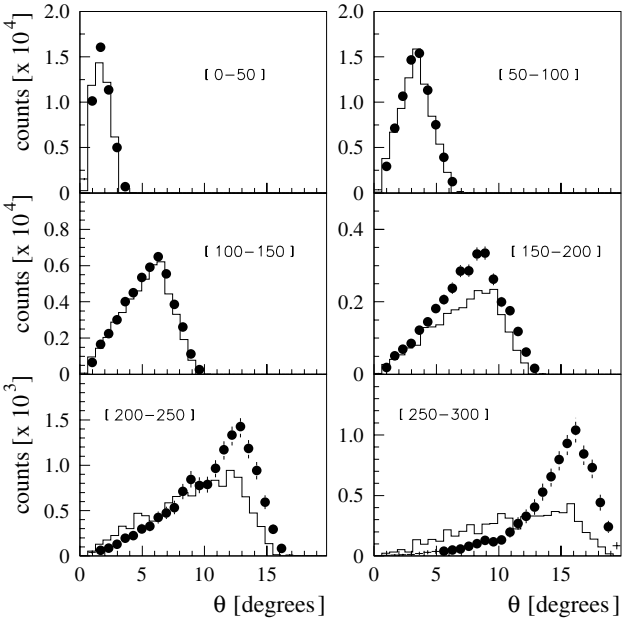

Fig. 8. Experimentally deduced angular distributions of the spectator proton in the laboratory system (dots with error bars) for indicated bins in Fermi momentum (given in MeV/c) in comparison with Monte Carlo data (solid histograms).

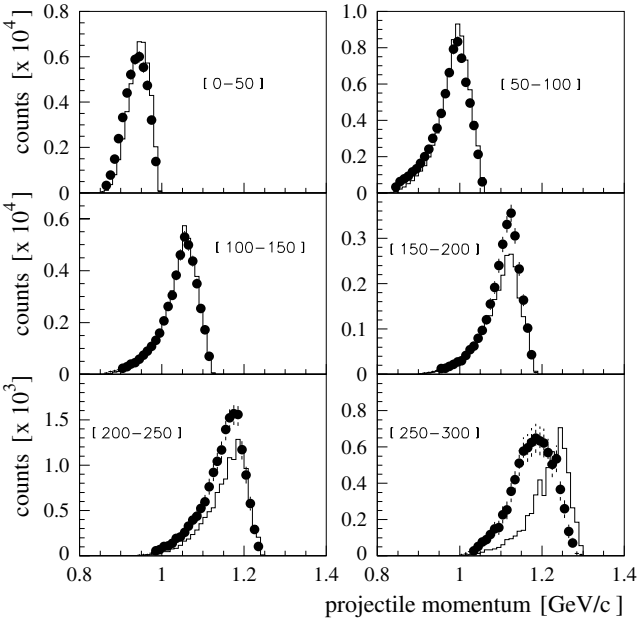

Fig. 9. Experimentally deduced effective neutron projectile momenta (dots with error bars) for indicated bins in Fermi momentum (given in MeV/c) in comparison with Monte Carlo data (solid histograms).

efficiency for charged particles in plastic scintillator material, the one for neutrons is energy dependent; for energies beyond 100 MeV it shows a downward slope of some 10%/70 MeV [32]. All experimental observables as, *e.g.*, θ_n, ϕ_n and β_n could easily be determined by choosing the center of the target as the beginning of the neutron track and taking as start time the TDC information supplied by either the elastically scattered proton or the spectator. Results are given in fig. 7. The histogram in the main frame shows the experimental angular p_s-distribution in the DCM system, the insert shows the squared missing mass (MM) distribution for all reconstructed 3-hit events: a strong peak around zero corresponding to the quasi-elastic scattering events, and a weak enhancement close to 0.02 GeV$^2/c^4$ stemming from the $dp \rightarrow pp\pi^- p_s$ reaction, where the pion escaped detection. The angular p_s-distribution was derived from events taken from a narrow window $\Delta MM^2/(\mathrm{GeV}^2/c^4) = [-0.005, +0.001]$ around the quasi-elastic peak; background events were subtracted by using a suitably normalized distribution at the far negative region. After correction for the varying neutron efficiency one arrives at the distribution shown in fig. 7 where indeed isotropy is observed.

The main goal for our investigation of the reaction $dp \rightarrow pp\pi^- p_s$ was to use it as a model case for spectator tagging, in general, and to derive some guidelines for future attempts where dp or pd reactions will be used as a substitute for studies of the pn-entrance channel. To this end, we divided the presently covered range in Fermi momentum up to 300 MeV/c into six momentum bins of width 50 MeV/c. We then checked for successively increasing Fermi momenta the agreement between experimental and Monte Carlo data for some selected observables such as spectator angular distribution (fig. 8) and effective neutron projectile momentum (fig. 9). The momentum ranges (in units of MeV/c) are listed in each panel.

The six consecutive bins represent 20.1, 33.8, 21.3, 13.5, 7.4, and 3.9% of the total yield, respectively, *i.e.* roughly 75% is found in the first three bins in the range up to $p_{Fermi} = 150$ MeV/c. A combined fit to these three bins (of spectator angle θ_s and neutron momentum) resulted in a reduced $\chi^2/n_f = 124.5/70$. No free parameter was used, instead we took the normalization factor as determined before (see sect. 2.3). When extending the fit to bins

of higher momenta, the χ^2-value increases rapidly, since yield as well as shape of corresponding distributions differ strongly. This result is due to various factors, the main one being that in the present experiment, where approximately 100 MeV in excess energy Q were covered, the simulation as well as the concurring acceptance corrections assumed purely phase space (s-wave) distributed events. This is definitely not true for the higher Q-values. Final-state interaction effects as were experimentally observed between the two reaction protons in the low-Q region or for large Fermi momenta between either one of these protons and the spectator were likewise not considered.

Another reason for the increasing differences between experimental data and Monte Carlo simulation stems from the fact, that it gets more and more difficult if not impossible to identify the spectator proton. In this case, however, we would like to argue, that when spectator and (one of) the reaction protons cannot be distinguished, it is no longer a quasi-free reaction. Instead the reaction has turned into one of a more collective nature.

We finally would like to comment on the results reported in ref. [16], where in general sizeable asymmetries were found in the spectator angular distributions of d- and ^{4}He-induced reactions on a proton target. The data collected at 3.34 GeV/c for the $dp \to pp\pi^- p_s$ reaction show a forward/backward asymmetry of roughly 1.6. As stated in the paper and acknowledged by one of its authors [33] the data are given in the "projectile nucleus rest frame (anti-laboratory frame)", which we understand to be identical to the DCM system used in the present study. In that case the published result is hard to understand. At this beam momentum a region in excess energy is covered where the cross-section for the quasi-free reaction is still slightly rising, at most almost constant, see, *e.g.*, the compilation given in [6]. For such a situation a result as in the present quasi-elastic scattering reaction, *i.e.*, an isotropic angular distribution was to be expected. The sizeable asymmetry [16], on the other hand, indicates already a decrease in cross-section, since backward-going neutrons seem to be favored.

4 Conclusion

We have measured the quasi-free $np \to pp\pi^-$ reaction in the range ΔQ = 10–100 MeV by means of a deuteron beam and spectator proton tagging. The data were analyzed in the framework of the spectator model and compared to Monte Carlo simulations. In order to check on the validity of the spectator model we used as input the known energy dependence of the cross-section as determined in recent experiments with a free neutron beam [6]. The momentum distribution of the bound neutron within the deuteron was calculated from the PARIS potential [25, 26] as well as the two-parameter Hulthen function [10]. From the good overall agreement between the experimental data and the Monte Carlo simulations we conclude that a deuteron beam can indeed be used as a valid substitute for a neutron beam provided that spectator detection is performed and only momenta below $p_{Fermi} = 150\,\mathrm{MeV}/c$ are taken into account in the analysis. Strictly speaking, our experiment demonstrates this finding only for backward emitted protons in the DCM system. Of course, these statements should also hold if a deuteron is used as a substitute for a neutron target. The information gathered from the spectator particle is the clue to such important quantities as effective beam momentum and direction, which both vary on an event-by-event basis. Using only one accelerator setting a range of approximately 100 MeV in excess energy can be covered, thus making excitation function measurements with tedious beam tuning obsolete. However, having a deuteron beam impinging on a proton target will only allow the study of low-threshold reactions. Even at COSY with its maximum beam momentum around 3.5 GeV/c, already the study of the next heavier non-strange meson, *i.e.*, η-production in the pn-entrance channel is only feasable by using a proton beam hitting a deuteron target with spectator protons in the few-MeV range. Suitable spectator detection devices have been developed for the two internal target experiments COSY-11 [14] and ANKE [15] which, when placed around 90°, cover up to 1π of the solid angle; first successful tests have already been carried out.

In an external target experiment the attempt to detect the low-energy spectator protons is almost in vain; yet two options are nevertheless available. The first one is to neglect spectator tagging at all and deduce averaged data only which may be feasable in cases where no strong energy variation of the cross-section is expected. More attractive, however, is the solution where one tries to reconstruct the four-momentum vector of the spectator proton by detection of all the remaining ejectiles. Several experiments along this line are planned for the large-acceptance spectrometer COSY-TOF, which in the past has been proven to be well suited for the investigation of many-particle reactions. The advantage of this method is that, in principle, no cut in spectator proton direction and hence no limitation in the range of the neutron momenta is given.

The help of the COSY crew in delivering a low-emittance deuteron beam is gratefully acknowledged. Helpful discussions with C. Hanhart, P. Moskal, R. Schleichert and C. Wilkin are very much appreciated. Financial support was granted by the German BMBF and by the FFE fund of the Forschungszentrum Jülich.

References

1. A.H. Rosenfeld, Phys. Rev. **96**, 130 (1954).
2. R. Handler, Phys. Rev. B **1380**, 1230 (1965) and references therein.
3. M. Kleinschmidt *et al.*, Z. Phys. A **298**, 253 (1980).
4. A. Bannwart *et al.*, Nucl. Phys. A **567**, 761 (1994).
5. M.G. Bachman *et al.*, Phys. Rev. C **52**, 495 (1995).
6. M. Daum *et al.*, Eur. Phys. J. C **23**, 43 (2002).
7. M. Daum *et al.*, Eur. Phys. J. C **25**, 55 (2002).
8. J.F. Crawford *et al.*, Phys. Rev. C **22**, 1184 (1979).
9. H. Braun *et al.*, Phys. Rev. D **2**, 488 (1970).

10. A. Fridman, Fortschr. Phys. **23**, 243 (1975).
11. F. Duncan *et al.*, Phys. Rev. Lett. **80**, 4390 (1998).
12. H. Hahn *et al.*, Phys. Rev. Lett. **82**, 2258 (1999).
13. R. Bilger *et al.*, Nucl. Instrum. Methods Phys. Res. A **457**, 6 (2001); J. Zlomanczuk, *4th International Conference STORI99*, AIP Conf. Proc. **512**, 43 (2000).
14. P. Moskal, nucl-ex/0110001 (2001); nucl-ex/0507033 (2005) and private communication.
15. I. Lehmann *et al.*, Nucl. Instrum. Methods Phys. Res. A **530**, 275 (2004) and private communication.
16. A. Dirner *et al.*, Eur. Phys. J. A **8**, 493 (2000).
17. COSY-TOF Collaboration (R. Bilger *et al.*), Phys. Lett. B **429**, 195 (1998).
18. COSY-TOF Collaboration (S. Abd El-Samad *et al.*), Eur. Phys. J. A **17**, 595 (2003).
19. COSY-TOF Collaboration (S. Abd El-Samad *et al.*), Phys. Lett. B **632**, 27 (2006).
20. A. Hassan *et al.*, Nucl. Instrum. Methods Phys. Res. A **425**, 403 (1999).
21. M. Wagner, PhD Thesis, Universität Erlangen-Nürnberg (2002).
22. M. Dahmen *et al.*, Nucl. Instrum. Methods Phys. Res. A **348**, 97 (1994).
23. A. Böhm *et al.*, Nucl. Instrum. Methods Phys. Res. A **443**, 238 (2000).
24. J. Kress, PhD Thesis, Universität Tübingen (2002).
25. M. Lacombe *et al.*, Phys. Lett. B **101**, 139 (1981).
26. C. Wilkin, private communication.
27. U. Zielinsky, PhD Thesis, Ruhr-Universität Bochum (1999).
28. Ł. Karsch, PhD Thesis, Technische Universität Dresden (2003).
29. GENBOD, CERN Program Library Long Write-up W515 (1993).
30. C. Besliu *et al.*, Yad. Fiz. **43**, 888 (1986).
31. T.J. Devlin *et al.*, Phys. Rev. D **8**, 136 (1973).
32. L. Karsch *et al.*, Nucl. Instrum. Methods Phys. Res. A **460**, 362 (2001) and references therein.
33. G. Martinska, private communication.